Effect of hydrothermal pretreatment on pyrolyzed sludge biochars for tetracycline adsorption

Weisheng Chen[a, 1], Baolong Zhao[a, b, 1, *], Yiping Guo[a], Yujie Guo[a], Zhihong Zheng[a], Tannaz Pak[c], Guoting Li[a, *]

a School of Environmental and Municipal Engineering, North China University of Water Resources and Electric Power, Zhengzhou 450046, China

b State Key Laboratory of Simulation and Regulation of Water Cycle in River Basin, Department of Water Resources (DWR), China Institute of Water Resources and Hydropower Research, Beijing, 100038, PR China

c School of Computing, Engineering & Digital Technologies, Teesside University, Borough Road, Middlesbrough, TS1 3BX, UK

***Corresponding author:** Tel: +86-371-69127538; Fax: +86-371-65790239;

E-mail: zbl_17@126.com (B.L. Zhao), lipsonny@163.cn (G.T. Li)

Foot note:[1] Authors contributed equally to this work.

Abstract

In this research, two biochars derived from activated sludge (wastewater treatment plant) are prepared by two different preparation processes for the comparative studies of tetracycline (TC) adsorption. One is the two-stage process, including hydrothermal pretreatment and subsequent high-temperature pyrolysis (HSBC-600), while the other is the direct pyrolysis method (PSBC-600). Various technologies are employed to characterize physicochemical properties and structural features of the two biochars. The results indicate that hydrothermal pretreatment can increase the specific surface area (133.4 and 114.6 m^2/g for HSBC-600 and PSBC-600) and pore volume (0.237 and 0.159 cm^3/g for HSBC-600 and PSBC-600) of biochar. At 298 K, the q_{max} on HSBC-600 and PSBC-600 achieves 116.9 and 89.3 mg/g, respectively. It is noted that the Freundlich isotherm and pseudo-second-order kinetic equations better describe the adsorption behavior, indicating that the adsorption of TC onto HSBC-600 and PSBC-600 is the multi-layer adsorption and involves chemical adsorption. The thermodynamic parameters reveal that the adsorption process is spontaneous and endothermic, causing an increase in the degree of disorder. All adsorption mechanisms may be consisted of pore filling, electrostatic force, hydrogen bond, and π-π interaction. The higher adsorption capacity of HSBC-600 could be attributed to the more adsorption sites provided from high specific surface area and pore volume, in which π-π interaction plays a major role.

Keywords: Adsorption; Biochar; Hydrothermal pretreatment; Sludge; Tetracycline

1. Introduction

Nowadays, pharmaceuticals and personal care products (PPCPs) often cause serious impact on the ecological environment due to the strong biological activity, optical rotation and chronic toxicity of these substance, being one of the emerging pollutants [1, 2]. Tetracyclines consisting of chlortetracycline, oxytetracycline, tetracycline and other derivatives are one of the important branches of PPCPs [3]. Tetracycline (TC), for example, is the second most consumed antibiotic in the world and often used as the antibacterial drug and growth promoter in agriculture and animal husbandry[4, 5]. However, approximately 80~90% of TC used in organisms are released into the outside of body in the form of parent compound and active metabolites through faeces and urine [6, 7]. Besides, the industrial wastewater discharged from many pharmaceutical factories that produce tetracycline contains a large amount of incompletely separated TC and its derivatives [8]. The existence of TC in the environment not only could cause water and soil pollution, but also threaten the health of humans, animals and plants through the food chain [6, 9]. Therefore, facing the serious problem of TC contamination, it is imperative to promote experimental research on the removal of TC remaining in the natural environment.

As previously reported, the traditional methods of TC removal include biological method, advanced oxidation method and adsorption method [10-12]. Generally, biological methods are prone to produce drug-resistant microorganisms. If they are discharged into the environment without proper treatment, they will have serious consequences for the ecological environment [13, 14]. The inability to treat

high-concentration antibiotic wastewater further restricts the application of biological methods [15]. Meanwhile, the removal of antibiotics by advanced oxidation processes may produce some undesired by-products, which may be higher toxic than their parental compounds [16]. Hence, adsorption is considered to be a promising and efficient treatment method compared to biological and advanced oxidation processes, with the main advantages of operation simplicity, high efficiency, low cost, and no toxic by-products [4, 17]. The focus of the adsorption method is the selection of the adsorbent, and carbonaceous materials consisting of activated carbon, biochar and graphite have received extensive attention due to their high porosity and excellent physical and chemical characteristics, etc [18-21]. Ji et al systematically investigated the adsorption ability of several carbonaceous materials for TC, which decreases in the pecking order: graphite/single-walled carbon nanotubes > multi-walled carbon nanotubes > activated carbon [19]. Although the above-mentioned carbonaceous materials have excellent properties, their preparation processes are relatively complex and high cost. As such, the preparation of biochar from waste biomass is a current research hotspot for the adsorption of pollutants. Sewage sludge containing heavy metals, pathogenic microorganisms and other pollutants, as by-product of sewage treatment plants, is produced in large quantities, and the output can reach 3.0×10^7 tons per year in China and 5.5×10^7 tons per year in Europe [17, 22]. If sludge is not disposed in a reasonable manner, it could cause serious damage to the ecosystem. The most common methods of sludge disposal are landfill and incineration, but they will occupy land resources, consume a lot of energy, and contaminate groundwater and air

[22, 23]. Considering that sludge contains a lot of organic matter, it is the suitable raw biomass to prepare biochar as adsorbent for the adsorption of pollutants, which could achieve the purpose of turning waste into treasure and treating waste with resource. Previous literatures have reported that sludge biochar achieved the efficient adsorption of tetracycline and ciprofloxacin, as well as heavy metal Pb(II) adsorption [17, 22].

Biochar is usually obtained by direct pyrolysis under oxygen-limited conditions or hydrothermal carbonization at low temperatures using waste-biomass as raw material [24]. Different preparation process can alter the physicochemical properties and structural characteristics of biochar. The hydrochar obtained by hydrothermal carbonization has abundant oxygen-containing functional groups. which can be used as active functional groups to interact with organic pollution containing aromatic rings through hydrogen bond or n-π interaction [17, 25]. However, direct-pyrolysis biochar can form higher porosity and more aromatic ring structures. The aromatic ring structure can be combined with aromatic organic pollutants through π-π interaction [26]. If different preparation methods are combined, the prepared biochar may combine the properties and advantages of each method. Notably, compared to the direct-pyrolysis biochar, pyrolyzed hydrochar shows higher specific surface area and carbon content, as well as lower ash content [27]. However, Tomul et al. has found the post-pyrolysis and pre-hydrothermal treatment have little effect on the specific surface area of the carbon material, but significantly change the adsorption performance of the carbon material. The maximum adsorption capacity is 800-800-PSB (324 mg/g) >

190-800-PSB (215 mg/g) > 800-PSB (105 mg/g) [24]. Zhang et al. has also found that further pyrolysis treatment for activated carbon promotes the adsorption of TC through π-π interaction [28]. Therefore, the physical-chemical properties and adsorption performance of the adsorbent may be changed obviously. However, the comparative studies on the adsorption of contaminants by sludge-based biochar synthesized by different preparation methods are scarcely reported.

In this study, sludge-based biochar is prepared by two different approaches. One is the direct-pyrolysis biochar, while the other one is a two-stage process, including hydrothermal carbonization and subsequent pyrolysis. Surface morphology, structural characteristics, surface functional groups and crystal structures of two carbon materials are analysed by various characterization techniques, which could reflect the effects of hydrothermal pretreatment for biochar. Moreover, using TC as the target pollutant, the adsorption performance of two sludge-based biochar is investigated. Combining with the characterization results of biochars before and after adsorption, it could further speculate the mechanism of the synthesized biochars for TC adsorption.

2. Materials and methods

2.1 Materials

Sewage sludge used for preparing biochar was provided from the Wang Xinzhuang sewage treatment plant (Zhengzhou, China). The obtained sludge was dried at 80 °C for 24 h, crushed, and sieved through 80 mesh for follow-up use. All chemical reagents were analytically pure, with tetracycline hydrochloride (TC) purchased from Shanghai Macklin Co. and other chemicals including NaOH, HCl, $NaNO_3$, $NaHCO_3$,

Na_2SO_4, and Na_3PO_4 bought from Kermel Chemical Reagent (Tianjin, China).

2.2 Preparation of sludge-based biochar

Comparatively, two different approaches were applied to prepare the sludge-based biochars. The first method was a two-stage process, including hydrothermal pretreatment and subsequent high-temperature pyrolysis. Firstly, 2 g of the above sludge powder and 20 mL of deionised water was mixed uniformly. The mixture was then put into the autoclave to heat (reaction conditions: 160 °C and 6 h). The obtained black solid was the sludge-based hydrochar. Then, the dried sludge-based hydrochar was pyrolyzed in the tube furnace under vacuum conditions (reaction conditions: 500~900 °C and 2 h). The final sludge-based biochar was recorded as HSBC-X (where X represents the pyrolysis temperature in the tube furnace). For comparison, the other sludge-based biochar was prepared by direct pyrolysis under the same conditions, and was recorded as PSBC-X.

2.3 Characterization of sludge-based biochar

Characterization methods of two biochars about the surface morphology, main surface elements, structural characteristics and surface functional groups are consistent with our previous literature report, which is presented in Text S1 [4].

2.4 Batch adsorption experiments

Adsorption experiments were carried out simultaneously to examine the effects of various reaction conditions. For experiments on the effect of initial pH (pH 3~11), coexisting anions and humic acid (HA) concentration, the reaction conditions are as following: 10 mg adsorbent, 25 ℃, 24 h, and 50 mL TC (20 mg/L) solution. For

kinetic studies, the reaction conditions are as following: 200 mg biochar, pH = 7, 25 ℃, and 1000 mL TC (20 mg/L) solution. For isotherm studies, the reaction conditions are as following: 10 mg biochar, pH = 7, 24 h, and 50 mL TC (10~200 mg/L) solution, and it was conducted at different temperatures (288, 298, and 308 K). In the above experiments, 0.1 M HCl or NaOH were applied to adjust solution pH. The samples were investigated by a UV752V spectrophotometer (360 nm) after filtering through the 0.45 μm membrane. It should be mentioned that several drops of HCl were added in the alkaline samples before colorimetric determination in order to exclude influence of hydrolysis. In addition, the TC adsorption capacity calculation equation, the adsorption kinetics equations, adsorption isotherms equations, thermodynamic equations, and their corresponding parameters are displayed in Text S2.

To study the renewability of adsorbent, NaOH, Ethanol, and thermal treatment regeneration method are applied. Detail procedures are conducted using our previously reported methods, which is provided in Text S3 [4].

3 Results and discussion

3.1 Effect of pyrolytic temperature

The effect of pyrolytic temperature on the TC adsorption is conducted by ranging the temperature from 500 to 900 ℃. As is displayed in Fig. S1, it shows that the adsorption capacity of TC onto the biochar (from HSBC-500 to HSBC-900) is significantly higher than that on the original hydrochar, indicating that high-temperature pyrolysis can change the properties of the hydrochar dramatically.

As the pyrolysis temperature varies from 500 to 600 ℃, the adsorption amount of HSBC-600 for TC exhibits a visible increase compared to HSBC-500, while it decreases gradually at higher temperature. The highest TC adsorption capacity (q_e = 54.3 mg/g) occurs at a pyrolysis temperature of 600 °C, with an increase of 56.0% compared to the pristine hydrochar (q_e = 34.8 mg/g). Actually, a suitable pyrolytic temperature can facilitate the development of pore structures within the biochar, forming more binding sites and thus contributing to the TC adsorption [17]. However, higher temperature may lead to the collapse of the pore structure, causing the decrease of adsorption capacity [29]. Considering cost-effectiveness, HSBC-600 and PSBC-600 are selected for comparative studies of TC adsorption in subsequent experiments.

3.2 Characterization of sludge-based biochar

Firstly, the yield of HSBC-600 and PSBC-600 is determined. The percentage of biochar yield is calculated by the mass ratio of the prepared biochars and the original sludge. It is noted that the yield of HSBC-600 and PSBC-600 is roughly 58.2% and 64.9%, respectively. The relatively high yield is conducive to the promotion and application of biochars in practice. Further, the surface morphology and element composition of HSBC-600 and PSBC-600 are assessed by the SEM/EDS, which is shown in Fig. 1. PSBC-600 has a blocky structure with some tiny spherical particles on the surface. In contrast, HSBC-600 pretreated by hydrothermal carbonization has a predominantly spherical morphology. A large number of spherical particles with smooth surfaces and relatively homogeneous dimensions accumulate and form pore

structures, which can facilitate the establishment of the higher porosity, thus promoting the adsorption performance for pollutants. Similar phenomenon is reported by other researchers [30]. In addition, the EDS qualitative analysis shows that the surfaces of both biochar contain not only abundant C and O elements, but also metallic elements such as Fe, Mg, Al and Ca. It is reported that complexion may occur between TC and metal cations (e.g. Ca^{2+}, Mg^{2+} and Fe^{3+}), thus metallic elements on the biochar surface may participate in the adsorption process of two biochars for TC [31, 32].

Fig. 1.

The N_2 adsorption/desorption analysis and corresponding structural properties of HSBC-600 and PSBC-600 are displayed in Fig. 2 and Table 1. The results can be found that the N_2 adsorption/desorption isotherms of two biochars correspond to the type IV pattern, indicating that the carbon materials are predominantly mesoporous internally. From Table 1, the specific surface area (133.4 and 114.6 m^2/g for HSBC-600 and PSBC-600) and pore volume (0.237 and 0.159 cm^3/g for HSBC-600 and PSBC-600) of biochar are increased by the hydrothermal pretreatment process. This can be explained that hydrochar produced from hydrothermal treatment is mainly amorphous carbon and has good self-binding properties, which is beneficial to further calcination to create more pore structures [33]. Wang et al. obtains a similar conclusion that hydrothermal pretreatment could obviously improve the specific surface area of SRC220-500 [34]. In addition, the pore size distribution shows that HSBC-600 and PSBC-600 are mainly mesoporous, with the average pore size of 6.16 and 5.24 nm, respectively. The pore structure of carbon material can obviously affect

the adsorption and mass transfer rate for adsorbate. According to the previous report, when the pore size of adsorbent is 1.7~3 times that of adsorbate, the adsorbent can efficiently adsorb the adsorbate [35]. The dimensions of TC (length, width and thickness) are 1.41, 0.46 and 0.82 nm, respectively [36]. Thus, both HSBC-600 and PSBC-600 have suitable pore-size range for adsorbing TC.

Fig. 2.

Table 1

The FTIR spectra of HSBC-600 and PSBC-600 is shown in Fig. 3a, which could be noted that the adsorption characteristic peaks of two biochars are similar, indicating that hydrothermal pretreatment does not cause significantly the change of main functional groups. This may be resulted from the mildness and stability of hydrothermal treatment, which is in line with previous studies reported [37]. Generally, the broad and strong absorption peaks can be seen in the range of 3300~3425 cm^{-1}, which are derived from the stretching vibration of -OH. It may come from the phenols, carboxyl groups or adsorbed water. The characteristic peak located around 1600 cm^{-1} is assigned to stretching vibrations of -C=O [22, 38]. The characteristic peaks intensity of -OH and -C=O after TC adsorption is significantly enhanced compared to the FTIR peaks of the original biochar before adsorption, suggesting that a large quantity of TC is adsorbed by HSBC-600 and PSBC-600. In addition, the characteristic peaks of other main functional groups can be found in the FTIR spectrum, including -C=C (1420~1450 cm^{-1}) stretching vibration in aromatic ring, -C-O (1050~1080 cm^{-1}) stretching vibration in ether or lactone group, CO_3^{2-}

(879 cm^{-1}) and -C-H stretching vibration on benzene ring (779 cm^{-1}) [26, 32]. Particularly, the -C=C from aromatic ring can provide π-electrons for π-π interactions with aromatic organic pollutants, facilitating TC adsorption [24]. When the characteristic peak is below 600 cm^{-1}, it corresponds to the metal-halogen (M-X) stretching vibration in organic or inorganic halogen compounds [39, 40].

The Raman patterns could be applied to determine the structural defect peculiarities and the degree of graphitization of the carbonaceous material. From Fig. 3b, it shows two typical adsorption bands (D-band and G-band) located near 1350 and 1591 cm^{-1}, respectively. The simultaneous appearance of the two adsorption bands indicates the coexistence of disordered amorphous carbon and ideal graphite lattices in the prepared carbon material [41]. In addition, the intensity ratio of the two typical adsorption bands is an indicator of the disorder or graphitization degree within the samples. The I_D/I_G values for both carbon materials are less than 1, indicating that the prepared carbon materials have low defectivity and a high degree of graphitization [42]. The similarity of the I_D/I_G values for HSBC-600 (I_D/I_G = 0.819) and PSBC-600 (I_D/I_G = 0.812) suggests that they have similar degree of graphitization.

Fig. 3.

Fig. S2 and Table S1 show the C1s high-resolution profiles of the two carbon materials, and the corresponding binding energy and chemical component distributions. It can be seen that the C1s high-resolution profile can be divided into four characteristic peaks with the corresponding chemical components, including -C-C, -C=C and -C-H (approximately 284.7 eV), -C-O (approximately 285.3 eV),

-C=O (approximately 286.5 eV), and CO_3^{2-} (approximately 289.1 eV) [43, 44]. Compared to PSBC-600, HSBC-600 has more oxygen-containing functional groups, which can bind to aromatic organic pollutants through hydrogen bond as π electron acceptors [45, 46]. This may be because of the hydrolysis, degradation, polycondensation, and aromatization during the hydrothermal carbonization stage [47].

The crystal structure of the carbon materials can be characterized by the XRD technique. The diffraction patterns of HSBC-600 and PSBC-600 are shown in Fig. S3. It can be noticed that they have similar diffraction peaks, indicating that the crystal structure of the carbon material has not been altered obviously by the hydrothermal pretreatment. The diffraction peak angles of 20.8°, 26.6°, 36.5°, 39.4°, 42.3°, 50.2°, 60.0° and 68.1° correspond to SiO_2 crystals in the material, while diffraction peak angles at 29.4°, 39.4° and 43.2° are the $CaCO_3$ crystals in accord with the FTIR and XPS analysis [48]. This suggests the abundant presence of SiO_2 and $CaCO_3$ crystals in both HSBC-600 and PSBC-600, which is in accord with previous reports [17]. The diffraction peak intensity of HSBC-600 is significantly higher than that of PSBC-600, indicating that the hydrothermal pretreatment is beneficial to enhance the crystallinity of the carbon material.

3.2 Effect of initial solution pH and coexisting anions

The surface charge of two biochars and the ionization degree of TC are driven by the initial solution pH [17]. Therefore, it is of great significance to explore the influence of the initial solution pH on the adsorption of TC. According to the

physicochemical properties of TC, it is an amphiphilic molecule (pK_a = 3.3, 7.7 and 9.7), and the ionic species at different pH are depicted in Fig. 4b. [49]. In addition, the zero point (pH_{PZC}) of biochar is the pH_{PZC} = 3.96 and pH_{PZC} = 3.94 for HSBC-600 and PSBC-600, respectively. At pH > pH_{PZC}, the surface of the biochar will be negatively charged by deprotonation, otherwise positively charged. From Fig. 4a, the adsorption capacity of TC by HSBC-600 and PSBC-600 shows a similar trend with the change of pH. Under near-neutral conditions, the negatively charged surfaces of HSBC-600 and PSBC-600 have a low electrostatic repulsion with TC existing mainly in the molecular state (H_3TC). The maximum adsorption capacities of TC by HSBC-600 and PSBC-600 occur at pH = 5 (q_e = 57.5 mg/g) and pH = 7 (q_e = 23.7 mg/g), respectively. In contrast, under acidic and basic conditions, the amount of TC adsorbed by both biochars decreases due to the increase of electrostatic repulsion, but some TC molecules are still adsorbed, which demonstrates that other interaction forces are also present between biochar and TC, including hydrogen bond or π-π interaction.

Furthermore, considering various anions ubiquitously present in natural water bodies, NO_3^-, SO_4^{2-}, HCO_3^- and PO_4^{3-} are investigated on the adsorption of TC by HSBC-600 and PSBC-600. The experiments are conducted with sodium salts for anions. As depicted in Fig. 4c and d, the addition of NO_3^- and SO_4^{2-} has no obvious effect on the adsorption of TC by HSBC-600. However, HCO_3^- and PO_4^{3-} have obvious inhibitory effect, and the amount of TC adsorbed decreases gradually with increasing anions concentration. After adding 0.05 M HCO_3^- and PO_4^{3-}, the adsorption

capacity of TC onto HSBC-600 decreases by 33.9% and 24.7%. On the one hand, this may be due to the increase of pH caused by the hydrolysis of HCO_3^- and PO_4^{3-}; on the other hand, it may be that HCO_3^- and PO_4^{3-} are more easily adsorbed on the surface of HSBC-600, and a large number of active sites are occupied by HCO_3^- and PO_4^{3-} [4, 50]. Differently, all four anions have some inhibitory effect on the adsorption of TC onto PSBC-600. Thus, hydrothermal pretreatment could make HSBC-600 more stable and widely adaptable.

Fig. 4.

3.3 Adsorption kinetics

The study of adsorption kinetics is a key method to evaluate adsorption rate and comprehend kinetic interactions between TC and two biochars. As reported in previous literature, the adsorption process of contaminants can be divided in two stages, including fast stage (initial 4 h) and slow stage [51]. Judged from Fig. 5a, the adsorption of over 90% TC occurs within the initial 2 h and the adsorption process is especially efficient, which could be because of high adsorbate concentration and reasonable pore structure of biochar [36]. After 2 h, the adsorption process enters slow phase because most of the adsorption sites have been occupied.

Typical kinetics models, containing the pseudo-first-order, pseudo-second-order and intra-particle diffusion kinetic models, are employed to simulate the adsorption experiment process, as displayed in Table 2 and Fig. 5a and b. It is noted that the R^2 of the pseudo-second-order kinetic model for both HSBC-600 and PSBC-600 higher than that of pseudo-first-order model. Meanwhile, the $q_{e,cal}$ values of 54.5 and 22.9 mg/g for

HSBC-600 and PSBC-600 obtained by the pseudo-second-order model are more approximate to their respective $q_{e,exp}$ values (54.5 and 23.7 mg/g). It has been suggested that chemisorption process accounts for the TC adsorption onto HSBC-600 and PSBC-600 while the rate-determining step may be chemical interaction, such as electron sharing or exchange [35]. In addition, the pseudo-second-order model parameter, $h = k_2 \cdot q_e^2$, can reflect the initial adsorption rate of TC. Compared to PSBC-600, the greater h value of HSBC-600 indicates that it has a higher initial adsorption rate, suggesting that hydrothermal pretreatment can affect the adsorption rate of biochar for TC [51].

In general, the adsorption rate and mechanism of adsorbate are controlled through three stages including the surface diffusion (stage 1) which represents that adsorbate crosses the phase interface resistance to reach the adsorbent surface, inner diffusion (stage 2) which represents that adsorbate enters the inner active site and pores of adsorbent from the adsorbent surface, and equilibrium phase (stage 3) which means that adsorption reaches the equilibrium stage [52]. As depicted in Fig. 5b, multi-linear portions between q_t and $t^{1/2}$ show that there are no linear portions passing the zero point, demonstrating that the rate-determining step could be controlled by surface diffusion and inner diffusion simultaneously. However, the intercepts of stage 2 for HSBC-600 and PSBC-600 are higher than those of stage 1, demonstrating the inner diffusion plays a major role in the rate-determining step [53]. Furthermore, the higher C_1 value of HSBC-600 indicates a greater contribution from its outer surface or transient adsorption than that of PSBC-600, which is involved in the larger surface

area of HSBC-600 [17].

Fig. 5.

Table 2

3.4 Adsorption isotherms

The adsorption isotherms of TC onto HSBC-600 and PSBC-600 are shown in Fig. 5c and d. It is found that the increasing temperature can facilitate the adsorption reaction, and the adsorption capacities of HSBC-600 and PSBC-600 increase by 71.7% and 41.5%, respectively, from 288 to 308 K. In addition, the Langmuir and Freundlich isotherm models are applied to fit the adsorption experimental results. Generally, the Langmuir isotherm model assumes that the adsorbent surface has energy-equivalent homogeneous adsorption site and combination with adsorbate on monolayer, while the Freundlich isotherm model has a hypothesis about the heterogeneous surface of adsorbent, and it is applicable to multilayer adsorption [41]. The simulated non-linear curves and related data are displayed in Fig. 5c and d and Table 3. By comparing their R^2 values, it is observed that best fitting isotherm model is the Freundlich isotherm with the R^2 value near 1.0. This indicates that adsorption mainly occurs heterogeneously via multilayer adsorption. Meanwhile, the Freundlich isotherm constant data, n, is calculated between 0.1~1, which implies that adsorption of TC at all temperatures is favorable [5]. Considering that R^2 values (0.943~0.983) of the Langmuir isotherm model are still great, it can reflect the q_{max} of adsorbent. From the Table 3**,** the maximal adsorption capacities at 298 K for HSBC-600 and PSBC-600 achieve 116.9 and 89.3 mg/g, respectively, which testifies that hydrothermal

pretreatment can significantly increase the adsorption capacity of TC, as well as HSBC-600 is quite acceptable for the practical application in water purification.

Table 3

3.5 Adsorption thermodynamics

To further investigate the adsorption mechanism, the adsorption thermodynamics of TC onto HSBC-600 and PSBC-600 are explored and the corresponding thermodynamic constant data are shown in Table 4. The positive value of ΔH_0 suggests that the adsorption is endothermic process. Similarly, some researchers conclude that the adsorption process of TC onto carbon materials occurs endothermally [17, 54]. Moreover, $\Delta G_0 < 0$ and $\Delta S_0 > 0$ manifest that the adsorption is spontaneous and the increasing in the degree of disorder. As the temperature goes up, the value of ΔG_0 decreases gradually, indicating that it is beneficial to the adsorption reaction at higher temperature. Meanwhile, the ΔG_0 values of HSBC-600 are more negative than those of PSBC-600, indicating that the adsorption reaction spontaneity of HSBC-600 is higher under the same conditions. This suggests that it is favorable for better adsorption capability for HSBC-600 [17]. Additionally, $\Delta H_0 < 40$ kJ/mol and -20 kJ/mol$< \Delta G_0 < 0$ reflect that the physisorption is involved with the adsorption of TC onto HSBC-600 and PSBC-600, such as hydrogen bond or pore filling [6].

Table 4

3.6 Possible adsorption mechanism

Adsorption of TC onto HSBC-600 and PSBC-600 causes obviously changes on the

textural properties and the surface functional groups which can be found by the BET and FTIR analysis before and after TC adsorption, respectively. As displayed in Table 1, HSBC-600 and PSBC-600 are mainly mesoporous. The monomer size of TC is 1.41, 0.46 and 0.81 nm (length, width and thickness), and the abundant mesopores can facilitate the diffusion of TC and reduce steric hindrance [36]. The S_{BET} and V_{Total} of both HSBC-600 and PSBC-600 decrease after TC adsorption, indicating that the TC molecules enter the interior of carbon materials with a strong shielding effect and blocking the pore channels. Particularly, their V_{Micro} reduces from 0.026 and 0.007 to 0.011 and 0.003 cm^3/g, respectively, which is a typical pore filling mechanism [24, 55]. Fig.2 c and d show that the pore size distribution of HSBC-600+TC and PSBC-600+TC shifts to the higher value compared to the pristine biochar, verifying the above conclusion. Furthermore, in combination with the data in Table 1, the hydrothermal pretreatment results in the higher specific surface area and pore volume for HSBC-600, thus providing more active sites to bind TC, which may be one of the reasons for the better adsorption capability of HSBC-600 compared to PSBC-600.

The FTIR spectrum is very sensitive to the variation of the functional groups. Therefore, the interaction between biochar and TC can be inferred from the wavenumber changes of the FTIR spectrum about biochar before and after adsorption. Generally, the aromatic ring structure of TC molecules can be closely combined with π electrons in the carbon material as π electron acceptor, which promoting the occurrence of π-π interaction [56]. From Fig. 3a, the wavenumber of -C=C in the FTIR spectrum of HSBC-600 shifts from 1422 to 1447 cm^{-1} following TC adsorption,

proving the existence of π-π interaction, which is consistent with the previous findings. However, the -C=C adsorption peak in the PSBC-600+TC spectrum has almost no shift compared to PSBC-600, indicating that π-π interaction has no obvious effect for absorbing TC by PSBC-600 [25]. Moreover, a pronounced shift (from 3340 to 3424 cm^{-1} for HSBC-600; and from 3317 to 3423 cm^{-1} for PSBC-600) and the increase in the intensity of -OH peak suggests the hydrogen bond involving in the TC adsorption process [54].

Summarily, FTIR and BET analysis reveal that the adsorption mechanisms of TC onto HSBC-600 and PSBC-600 include pore filling, π-π interaction, and hydrogen bond. Besides, electrostatic force is also a key factor. However, compared to the PSBC-600, the higher adsorption capacity of HSBC-600 for TC could be due to the more adsorption sites provided from high specific surface area and pore volume, in which π-π interaction plays a major role.

3.7 Effects of humic concentration

Macromolecular organic matter-humic acids originated from the decompose of the dead animals and plants in nature is widely distributed in natural water bodies, which may affect the adsorption efficiency of TC onto HSBC-600 and PSBC-600. The Fig. S4 shows the effect of different concentrations of HA (0~10 mg/L), which manifests that the amount of TC adsorbed by HSBC-600 gradually increases when the HA concentration is increasing. Generally, HA can be bound to the surface of HSBC-600 by hydrogen bond, electrostatic force, and π-π interactions [57]. The HA adsorbed can play a bridging role to increase the adsorption site on the surface of

HSBC-600, which may be combined with a large amount of TC [58]. Thus, HSBC-600 retains higher adsorption efficiency of TC even though the presence of HA. However, the adsorption capacity of TC onto PSBC-600 at the different concentration of HA has a different trend compared to the HSBC-600. When HA is at the low concentration, the adsorption capacity of TC decreases obviously. This may be because of the adsorption sites competition between TC and HA. However, there is a slight increasing in the adsorption capacity of TC as the concentration of HA increases (> 6 mg/L). This may be because that HA acts as a bridge to interact with TC. Similar phenomenon is found by Zhou et al., and the TC adsorption capacity of TC on activated carbon loaded Fe_3O_4 decreases when the concentration of HA is 2~6 mg/L HA. As the increasing of HA concentration to 8~10 mg/L, it facilitates the adsorption of TC [50].

3.8 Regeneration experiments

Here, the renewability of HSBC-600 and PSBC-600 is investigated using NaOH, ethanol, and thermal treatment. From Fig. S5., NaOH and thermal treatment methods have good regeneration effects on HSBC-600 and PSBC-600. After four regenerations, the adsorption capacity of TC by HSBC-600 decreases from 54.8 to 35.4 (NaOH treatment) and 49.8 mg/g (thermal treatment), and the adsorption capacity of TC by PSBC-600 decreases from 23.3 to 17.5 (NaOH treatment) and 18.5 mg/g (thermal treatment), respectively, indicating that the adsorption site of HSBC-600 and PSBC-600 cannot be completely reversed. Although the adsorption capacity of HSBC-600 after recycling has declined, its adsorption capacity can still be suitable for

actual wastewater treatment.

4. Conclusions

In this study, the effect of hydrothermal pretreatment for the physicochemical properties and adsorption behavior of biochar is explored. Results show that hydrothermal pretreatment can increase the specific surface area (133.4 and 114.6 m^2/g for HSBC-600 and PSBC-600), pore volume (0.237 and 0.159 cm^3/g for HSBC-600 and PSBC-600), the content of oxygen-containing functional groups and crystallinity of biochar, which contribute to TC adsorption. The experimental data of initial solution pH indicates that electrostatic force plays an important role. The higher R^2 values (0.990~0.994) of the pseudo-second-order kinetic model indicate that chemisorption process accounts for the TC adsorption onto HSBC-600 and PSBC-600. Meanwhile, best fitting isotherm model is the Freundlich isotherm, indicating that the adsorption of TC by the two biochars is multi-molecular layer adsorption. The thermodynamic constant data confirm that the TC adsorption onto both HSBC-600 and PSBC-600 is spontaneous and endothermic, causing an increase in the degree of disorder. In addition, all adsorption mechanisms may be comprised of pore filling, electrostatic force, hydrogen bond, and π-π interaction, while π-π interaction is a key contributor to the higher TC adsorption capacity onto HSBC-600 compared to PSBC-600.

Credit authorship contribution statement

Weisheng Chen: Investigation, data analysis, writing–original draft. **Baolong Zhao**: Investigation, validation, writing, collection, editing. **Yiping Guo**: Investigation, methodology, data analysis, plots etc. **Yujie Guo**: Data analysis,

resources, plots etc. **Zhihong Zheng**: Data analysis, assistance to Investigation. **Tannaz Pak:** Reviewing/rewriting the manuscript and contribution to improving the revised version from scientific, language, and presentation perspectives. **Guoting Li**: Project administration, assistance to Investigation, review, correction, editing.

Declaration of competing interests

The authors declare that they have no known competing financial interests or personal relationships that could have appeared to influence the work reported in this paper.

Acknowledgment

The Authors thank for financial support from the grant Advanced manufacturing of biochar in UK/China/Malaysia/Nigeria (British Council, UK-China-BRI Countries Education Partnership Initiative, 2019), the China National Natural Science Foundation (Grant No. 51378205), and the Natural Science Foundation of Henan (Grant No. 182300410136).

References

[1] E.N. Evgenidou, I.K. Konstantinou, D.A. Lambropoulou, Occurrence and removal of transformation products of PPCPs and illicit drugs in wastewaters: A review, Sci. Total Environ. 505 (2015) 905-926.

[2] I. Tamura, Y. Yasuda, K.-i. Kagota, S. Yoneda, N. Nakada, V. Kumar, Y. Kameda, K. Kimura, N. Tatarazako, H. Yamamoto, Contribution of pharmaceuticals and personal care products (PPCPs) to whole toxicity of water samples collected in effluent-dominated urban streams, Ecotoxicol. Environ. Saf. 144 (2017) 338.

[3] J.F. Liu, H. Lin, Y.B. Dong, Y.H. He, W. Liu, Y.y. Shi, The effective adsorption of tetracycline onto MoS_2@Zeolite-5: Adsorption behavior and interfacial mechanism, J.

Environ. Chem. Eng. 9(2) (2021) 105912.

[4] Z.H. Zheng, B.L. Zhao, Y.P. Guo, Y.J. Guo, T. Pak, G.T. Li, Preparation of mesoporous batatas biochar via soft-template method for high efficiency removal of tetracycline, Sci. Total Environ. 787 (2021) 147397.

[5] J.L. Liu, B.Q. Zhou, H. Zhang, J. Ma, B. Mu, W.B. Zhang, A novel biochar modified by Chitosan-Fe/S for tetracycline adsorption and studies on site energy distribution, Bioresour. Technol. 294 (2019) 122152.

[6] Z.T. Zeng, S.J. Ye, H.P. Wu, R. Xiao, G.M. Zeng, J. Liang, C. Zhang, J.F. Yu, Y.L. Fang, B. Song, Research on the sustainable efficacy of g-MoS_2 decorated biochar nanocomposites for removing tetracycline hydrochloride from antibiotic-polluted aqueous solution, Sci. Total Environ. 648 (2019) 206-217.

[7] S.M. Mirsoleimani-azizi, P. Setoodeh, S. Zeinali, M.R. Rahimpour, Tetracycline antibiotic removal from aqueous solutions by MOF-5: Adsorption isotherm, kinetic and thermodynamic studies, J. Environ. Chem. Eng. 6(5) (2018) 6118-6130.

[8] R. Changotra, H. Rajput, J.P. Guin, L. Varshney, Hybrid coagulation, gamma irradiation and biological treatment of real pharmaceutical wastewater, Chem. Eng. J. 370 (2019) 595-605.

[9] Y.Y. Zhou, Y.Z. He, Y.Z. He, X.C. Liu, B. Xu, J.F. Yu, C.H. Dai, A.Q. Huang, Y. Pang, L. Luo, Analyses of tetracycline adsorption on alkali-acid modified magnetic biochar: site energy distribution consideration, Sci. Total Environ. 650 (2019) 2260-2266.

[10] D.L. Cheng, H.H. Ngo, W.S. Guo, Y.W. Liu, J.L. Zhou, S.W. Chang, D.D. Nguyen,

X.T. Bui, X.B. Zhang, Bioprocessing for elimination antibiotics and hormones from swine wastewater, Sci. Total Environ. 621 (2018) 1664-1682.

[11] A. Mandal, K. Ojha, A.K. De, S. Bhattacharjee, Removal of catechol from aqueous solution by advanced photo-oxidation process, Chem. Eng. J. 102(2) (2004) 203-208.

[12] Y. Dai, J. Li, D. Shan, Adsorption of tetracycline in aqueous solution by biochar derived from waste Auricularia auricula dregs, Chemosphere 238 (2019) 124432.

[13] F.B. Yin, H.M. Dong, W.Q. Zhang, Z.P. Zhu, B. Shang, Antibiotic degradation and microbial community structures during acidification and methanogenesis of swine manure containing chlortetracycline or oxytetracycline, Bioresour. Technol. 250 (2018) 247-255.

[14] S.W. Joshua, E. Garner, A. Pruden, S.A. Diana, Occurrence and transformation of veterinary antibiotics and antibiotic resistance genes in dairy manure treated by advanced anaerobic digestion and conventional treatment methods, Environ. Pollut. 236 (2018) 764-772.

[15] X. Huang, J.L. Zheng, C.X. Liu, L. Liu, Y.H. Liu, H.Y. Fan, T.F. Zhang, Performance and bacterial community dynamics of vertical flow constructed wetlands during the treatment of antibiotics-enriched swine wastewater, Chem. Eng. J. 316 (2017) 727-735.

[16] S. Patel, S.K. Majumder, P. Das, P. Ghosh, Ozone microbubble-aided intensification of degradation of naproxen in a plant prototype, J. Environ. Chem. Eng. 7(3) (2019) 103102.

[17] Y.F. Ma, M. Li, P. Li, L. Yang, L. Wu, F. Gao, X.B. Qi, Z.L. Zhang, Hydrothermal

synthesis of magnetic sludge biochar for tetracycline and ciprofloxacin adsorptive removal, Bioresour. Technol. 319 (2021) 124199.

[18] W.P. Xiong, G.M. Zeng, Z.H. Yang, Y.Y. Zhou, C. Zhang, Adsorption of tetracycline antibiotics from aqueous solutions on nanocomposite multi-walled carbon nanotube functionalized MIL-53 (Fe) as new adsorbent, Sci. Total Environ. 627 (2018) 235-244.

[19] L.L. Ji, W. Chen, L. Duan, D.Q. Zhu, Mechanisms for strong adsorption of tetracycline to carbon nanotubes: a comparative study using activated carbon and graphite as adsorbents, Environ. Sci. Technol. 43(7) (2009) 2322-2327.

[20] T.H. Tran, H.H. Le, T.H. Pham, D.T. Nguyen, D.D. La, S.W. Chang, S.M. Lee, W.J. Chung, D.D. Nguye, Comparative study on methylene blue adsorption behavior of coffee husk-derived activated carbon materials prepared using hydrothermal and soaking methods, J. Environ. Chem. Eng. 9(2) (2021) 105362.

[21] M. Stylianou, A. Christou, C. Michael, A. Agapiou, P. Papanastasiou, D. Fatta-Kassinos, Adsorption and removal of seven antibiotic compounds present in water with the use of biochar derived from the pyrolysis of organic waste feedstocks, J. Environ. Chem. Eng. 9(5) (2021) 105868.

[22] J.J Zhang, J.G. Shao, Q.Z. Jin, Z.Q. L, X. Zhang, Y.Q. Chen, S.H. Zhang, H.P. Chen, Sludge-based biochar activation to enhance Pb(II) adsorption, Fuel. 252 (2019) 101-108.

[23] M. Kacprzak, E. Neczaj, K. Fijakowski, A. Grobelak, B.R. Singh, Sewage sludge disposal strategies for sustainable development, Environ. Res. 156 (2017) 39-46.

[24] F. Tomul, Y. Arslan, B. Kabak, D. Trak, E. Kendüzler, E.C. Lima, H.N. Tran, Peanut shells-derived biochars prepared from different carbonization processes: Comparison of characterization and mechanism of naproxen adsorption in water, Sci. Total Environ. 726 (2020) 137828.

[25] H.N. Tran, S.J. You, H.P. Chao, Fast and efficient adsorption of methylene green 5 on activated carbon prepared from new chemical activation method, J. Environ. Manage. 188 (2017) 322-336.

[26] J.W. Jin, Y.N. Li, J.Y. Zhang, S.C. Wu, Y.C. Cao, P. Liang, J. Zhang, M.H. Wong, M.Y. Wang, S.D. Shan, Influence of pyrolysis temperature on properties and environmental safety of heavy metals in biochars derived from municipal sewage sludge, J. Hazard. Mater. 320 (2016) 417-426.

[27] M.P. Olszewski, S.A. Nicolae, P.J. Arauzo, M.-M. Titirici, A. Kruse, Wet and dry? Influence of hydrothermal carbonization on the pyrolysis of spent grains J. Clean. Prod. 260 (2020) 121101.

[28] D.F. Zhang, P.L. Huo, L. Wei, Behavior of phenol adsorption on thermal modified activated carbon, Chin. J. Chem. Eng. 24(4) (2016) 446-452.

[29] H.B. Li, X.L. Dong, E.B.d. Silva, L.M.d. Oliveira, Y.S. Chen, L.Q. Ma, Mechanisms of metal sorption by biochars: Biochar characteristics and modifications, Chemosphere 178 (2017) 466-478.

[30] H.N. Tran, F. Tomul, H.T.H. Nguyen, D.T. Nguyen, E.C. Lima, G.T. Le, C.-T. Chang, V. Masindi, S.H. Woo, Innovative spherical biochar for pharmaceutical removal from water: Insight into adsorption mechanism, J. Hazard. Mater. 394 (2020) 122255.

[31] R. Anton-Herrero, C. Garcia-Delgado, M. Alonso-Izquierdo, G. Garcia-Rodriguez, J. Cuevas, E. Eymar, Comparative adsorption of tetracyclines on biochars and stevensite: Looking for the most effective adsorbent, Appl. Clay Sci. 160 (2018) 162-172.

[32] Y.K. Choi, T.R. Choi, R. Gurav, S.K. Bhatia, Y.H. Yang, Adsorption behavior of tetracycline onto *Spirulina* sp. (microalgae)-derived biochars produced at different temperatures, Sci. Total Environ. 710 (2020) 136282.

[33] S. Román, J.M. Valente Nabais, B. Ledesma, J.F. González, C. Laginhas, M.M. Titirici, Production of low-cost adsorbents with tunable surface chemistry by conjunction of hydrothermal carbonization and activation processes, Micropor. Mesopor. Mat. 165 (2013) 127-133.

[34] X. Wang, Q. Chi, X. Liu, Y. Wang, Influence of pyrolysis temperature on characteristics and environmental risk of heavy metals in pyrolyzed biochar made from hydrothermally treated sewage sludge, Chemosphere 216 (2019) 698-706.

[35] L.L. Yan, Y. Liu, Y.D. Zhang, S. Liu, C.X. Wang, W.T. Chen, C. Liu, Z.L. Chen, Y. Zhang, $ZnCl_2$ modified biochar derived from aerobic granular sludge for developed microporosity and enhanced adsorption to tetracycline, Bioresour. Technol. 297 (2020) 122381.

[36] L. Tang, J.F. Yu, Y. Pang, G.M. Zeng, Y.C. Deng, J.J. Wang, X.Y. Ren, S.J. Ye, B. Peng, H.P. Feng, Sustainable efficient adsorbent: Alkali-acid modified magnetic biochar derived from sewage sludge for aqueous organic contaminant removal, Chem. Eng. J. 336 (2018) 160-169.

[37] L. Bahcivanji, G. Gascó, J. Paz-Ferreiro, A. Méndez, The effect of post-pyrolysis treatment on waste biomass derived hydrochar, Waste Manage. 106 (2020) 55-61.

[38] L. Delgado-Moreno, S. Bazhari, G. Gasco, A. Méndez, M. El Azzouzi, E. Romero, New insights into the efficient removal of emerging contaminants by biochars and hydrochars derived from olive oil wastes, Sci. Total Environ. 752 (2021) 141838.

[39] M.K. Hossain, V. Strezov, K.Y. Chan, A. Ziolkowski, P.F. Nelson, Influence of pyrolysis temperature on production and nutrient properties of wastewater sludge biochar, J. Environ. Manage. 92(1) (2011) 223-228.

[40] H.J. Huang, T. Yang, F.Y. Lai, G.Q. Wu, Co-pyrolysis of sewage sludge and sawdust/rice straw for the production of biochar, J. Anal. Appl. Pyrol. 125 (2017) 61-68.

[41] G. Prasannamedha, P. Senthil Kumar, R. Mehala, T.J. Sharumitha, D. Surendhar, Enhanced adsorptive removal of sulfamethoxazole from water using biochar derived from hydrothermal carbonization of sugarcane bagasse, J. Hazard. Mater. 407(1) (2021) 124825.

[42] P. Pachfule, D. Shinde, M. Majumder, Q. Xu, Fabrication of carbon nanorods and graphene nanoribbons from a metal–organic framework, Nat. Chem. (2016).

[43] J.G. Shao, J.J. Zhang, X. Zhang, Y. Feng, H. Zhang, S.H. Zhang, H.P. Chen, Enhance SO_2 adsorption performance of biochar modified by CO_2 activation and amine impregnation, Fuel 224 (2018) 138-146.

[44] Y.q. Chen, B. Liu, H.p. Yang, X.h. Wang, X. Zhang, H.p. Chen, Generalized two-dimensional correlation infrared spectroscopy to reveal the mechanisms of

lignocellulosic biomass pyrolysis, P. Combust. Inst. 37(3) (2018) 3013-3021.

[45] J.Y. Song, S.H. Jhung, Adsorption of pharmaceuticals and personal care products over metal-organic frameworks functionalized with hydroxyl groups: Quantitative analyses of H-bonding in adsorption, Chem. Eng. J. 322 (2017) 366-374.

[46] Y.Q. Wang, C.Y. Lin, X.T. Liu, W.B. Ren, X.K. Huang, M.C. He, W. Ouyang, Efficient removal of acetochlor pesticide from water using magnetic activated carbon: Adsorption performance, mechanism, and regeneration exploration, Sci. Total Environ. 778 (2021) 146353.

[47] B. Ibrahim, M. Schlegel, N. Kanswohl, Investigation of applicability of wetland biomass for producing biochar by hydrothermal carbonization (HTC), Landbauforsch. Volk. 64(2) (2014) 119-124.

[48] Y.X. Liu, S. Yao, Y.Y. Wang, H.H. Lu, S.K. Brar, S.M. Yang, Bio- and hydrochars from rice straw and pig manure: Inter-comparison, Bioresour. Technol. 235 (2017) 332-337.

[49] Y.Y. Zhou, X.C. Liu, Y.J. Xiang, P. Wang, J.C. Zhang, F.F. Zhang, J.H. Wei, L. Luo, M. Lei, L. Tang, Modification of biochar derived from sawdust and its application in removal of tetracycline and copper from aqueous solution: Adsorption mechanism and modelling, Bioresour. Technol. 245 (2017) 266-273.

[50] J. Zhou, F. Ma, H. Guo, Adsorption behavior of tetracycline from aqueous solution on ferroferric oxide nanoparticles assisted powdered activated carbon, Chem. Eng. J. 384 (2020) 123290.

[51] F. Wang, W.L. Sun, W.Y. Pan, N. Xu, Adsorption of sulfamethoxazole and

17β-estradiol by carbon nanotubes/$CoFe_2O_4$ composites, Chem. Eng. J. 274 (2015) 17-29.

[52] Y. Li, M.A. Taggart, C. Mckenzie, Z.l. Zhang, Y.l. Lu, S. Pap, S. Gibb, Utilizing low-cost natural waste for the removal of pharmaceuticals from water: Mechanisms, isotherms and kinetics at low concentrations, J. Clean. Prod. 227(1) (2019) 88-97.

[53] Y.Y. Sun, H. Li, G. Li, B.Y. Gao, Q.Y. Yue, X.B. Li, Characterization and ciprofloxacin adsorption properties of activated carbons prepared from biomass wastes by H_3PO_4 activation, Bioresour. Technol. 217 (2016) 239-244.

[54] W. Wang, M. Gao, M.B. Cao, J.M. Dan, H.B. Yang, Self-propagating synthesis of Zn-loaded biochar for tetracycline elimination, Sci. Total Environ. 759 (2021) 143542.

[55] O. Paunovic, S. Pap, S. Maletic, M.A. Taggart, N. Boskovic, M.T. Sekulic, Ionisable emerging pharmaceutical adsorption onto microwave functionalised biochar derived from novel lignocellulosic waste biomass, J. Colloid Inter. Sci. 547 (2019) 350-360.

[56] K. Yang, B.S. Xing, Adsorption of organic compounds by carbon nanomaterials in aqueous phase: Polanyi theory and its application, Chem. Rev. 110 (2010) 5989-6008.

[57] Y.J. Xiang, Z.Y. Xu, Y.Y. Wei, Y.Y. Zhou, X. Yang, Y. Yang, J. Yang, J.C. Zhang, L. Luo, Z. Zhou, Carbon-based materials as adsorbent for antibiotics removal: Mechanisms and influencing factors, J. Environ. Manage. 237 (2019) 128-138.

[58] Y.P. Zhao, J.J. Geng, X.R. Wang, X.Y. Gu, S.X. Gao, Adsorption of tetracycline onto goethite in the presence of metal cations and humic substances, J. Colloid Inter. Sci. 361(1) (2011) 247-251.

Figure Captions

Fig. 1. SEM/EDS analysis of biochar (a) HSBC-600 and (b) PSBC-600.

Fig. 2. Nitrogen adsorption/desorption isotherms of (a) HSBC-600 and (b) PSBC-600 before and after adsorption of TC; pore size distribution of (c) HSBC-600 and (d) PSBC-600 before and after adsorption of TC.

Fig. 3. (a) FTIR spectrum of HSBC-600 and PSBC-600 before and after adsorption of TC, and (b) Raman patterns of HSBC-600 and PSBC-600.

Fig. 4. (a) Effect of initial solution pH; (b) the species of TC at different pH; the effect of coexisting anions for (c) HSBC-600 and (d) PSBC-600.

Fig. 5. (a) The pseudo-first-order, pseudo-second-order and (b) intra-particle diffusion kinetic models for TC adsorption; the Langmuir and Freundlich isotherm models for TC adsorption onto (c) HSBC-600 and (d) PSBC-600.

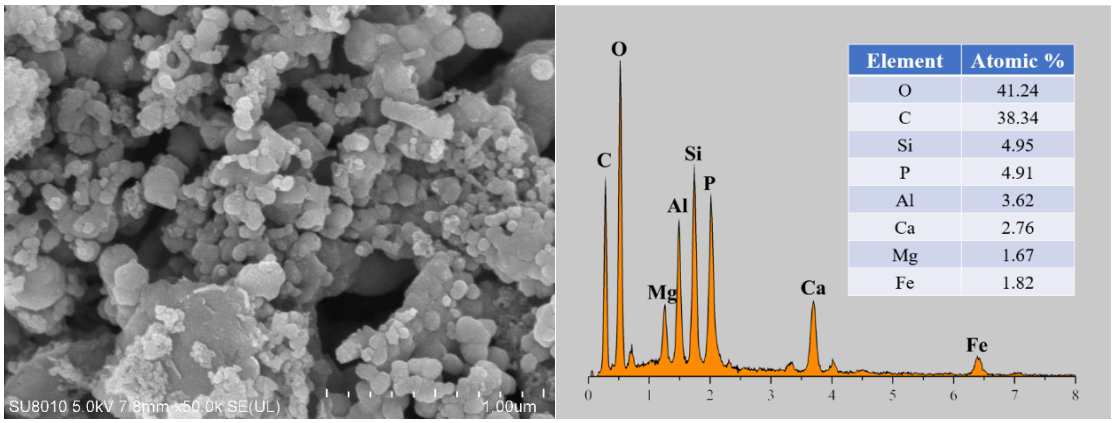

Element	Atomic %
O	41.24
C	38.34
Si	4.95
P	4.91
Al	3.62
Ca	2.76
Mg	1.67
Fe	1.82

(a)

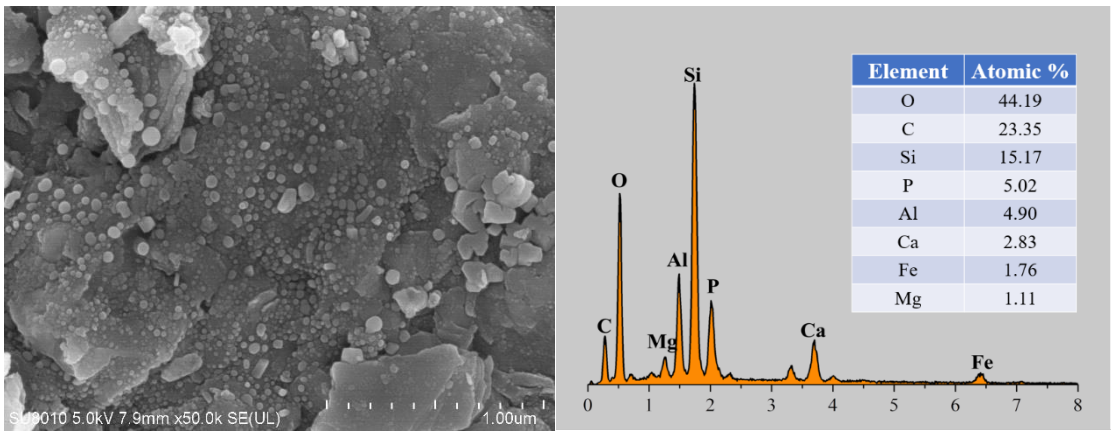

Element	Atomic %
O	44.19
C	23.35
Si	15.17
P	5.02
Al	4.90
Ca	2.83
Fe	1.76
Mg	1.11

(b)

Fig. 1.

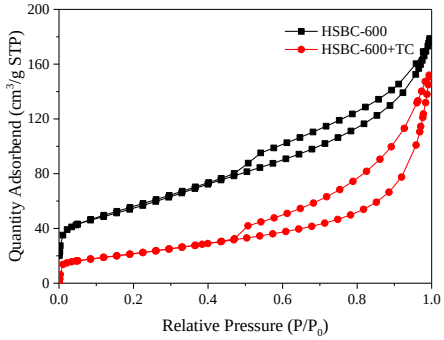
HSBC-600
HSBC-600+TC
Quantity Adsorbend (cm3/g STP)
Relative Pressure (P/P0)

(a)

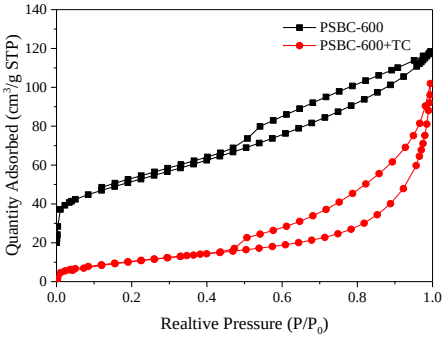
PSBC-600
PSBC-600+TC
Quantity Adsorbed (cm3/g STP)
Realtive Pressure (P/P0)

(b)

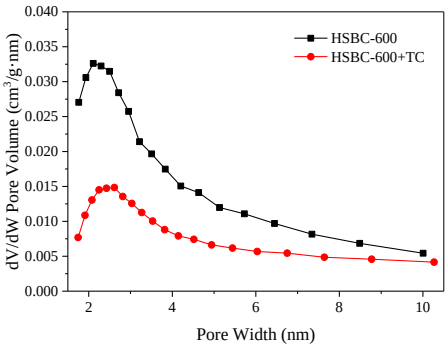
HSBC-600
HSBC-600+TC
dV/dW Pore Volume (cm3/g·nm)
Pore Width (nm)

(c)

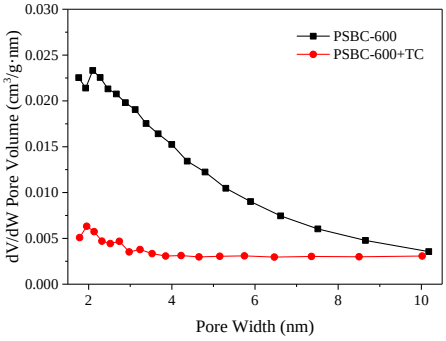
PSBC-600
PSBC-600+TC
dV/dW Pore Volume (cm3/g·nm)
Pore Width (nm)

(d)

Fig. 2.

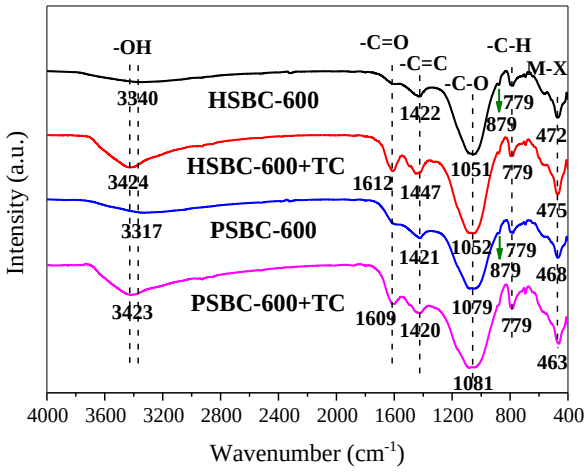
-OH
-C=O
-C=C
-C-H
-C-O
M-X
3340
HSBC-600
1422
779
879
472
1051
3424
HSBC-600+TC
1612
1447
779
475
3317
PSBC-600
1052
1421
779
879
468
3423
PSBC-600+TC
1609
1420
1079
779
463
1081
Intensity (a.u.)
4000 3600 3200 2800 2400 2000 1600 1200 800 400
Wavenumber (cm-1)

(a)

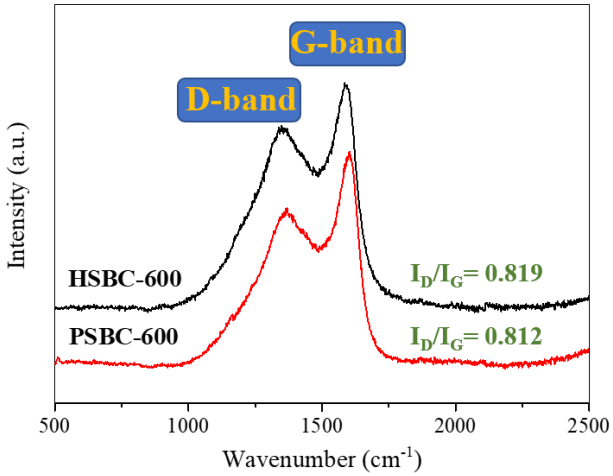
G-band
D-band
Intensity (a.u.)
HSBC-600
ID/IG= 0.819
PSBC-600
ID/IG= 0.812
500 1000 1500 2000 2500
Wavenumber (cm-1)

(b)

Fig. 3.

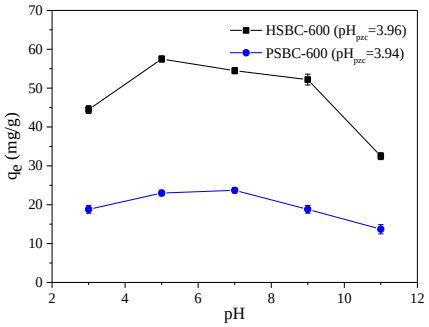
HSBC-600 (pHpzc=3.96)
PSBC-600 (pHpzc=3.94)
qe (mg/g)
pH

(a)

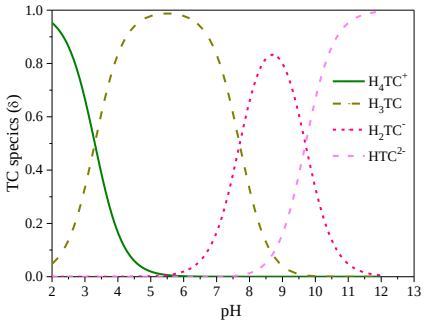
H4TC+
H3TC
H2TC-
HTC2-
TC species (δ)
pH

(b)

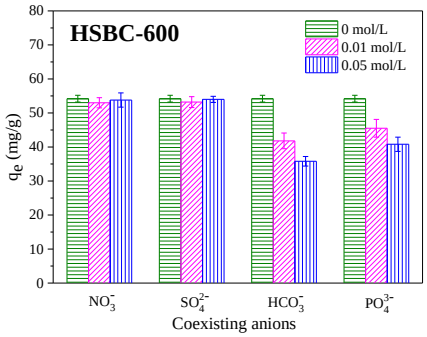
HSBC-600
0 mol/L
0.01 mol/L
0.05 mol/L
qe (mg/g)
NO3-
SO42-
HCO3-
PO43-
Coexisting anions

(c)

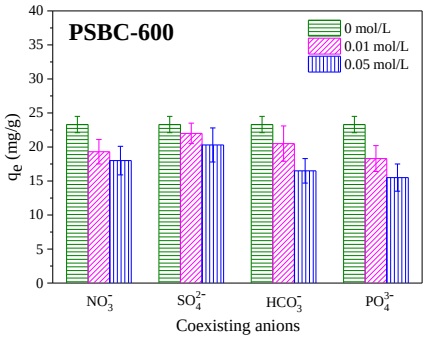
PSBC-600
0 mol/L
0.01 mol/L
0.05 mol/L
qe (mg/g)
NO3-
SO42-
HCO3-
PO43-
Coexisting anions

(d)

Fig. 4.

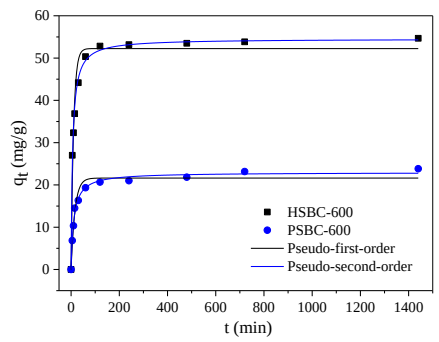
HSBC-600
PSBC-600
Pseudo-first-order
Pseudo-second-order
q_t (mg/g)
t (min)

(a)

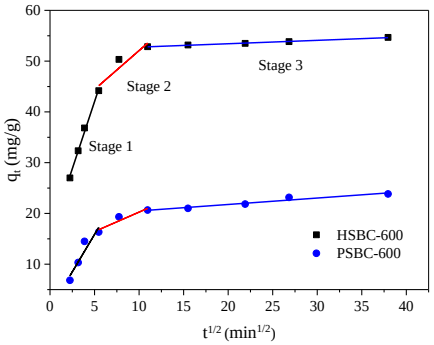
Stage 1
Stage 2
Stage 3
HSBC-600
PSBC-600
q_t (mg/g)
$t^{1/2}$ ($min^{1/2}$)

(b)

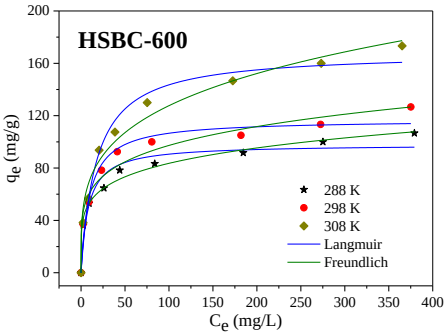
HSBC-600
288 K
298 K
308 K
Langmuir
Freundlich
q_e (mg/g)
C_e (mg/L)

(c)

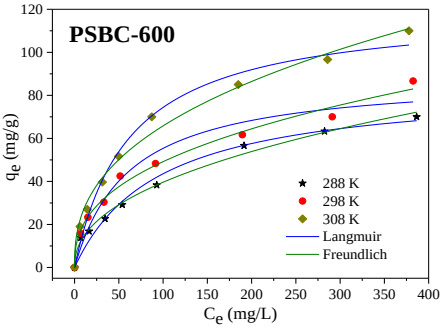
PSBC-600
288 K
298 K
308 K
Langmuir
Freundlich
q_e (mg/g)
C_e (mg/L)

(d)

Fig .5.

Table 1 Textural properties of HSBC-600 and PSBC-600 before and after adsorption of TC.

	Unit	HSBC-600		PSBC-600	
		Before adsorption	After adsorption	Before adsorption	After adsorption
S_{BET}	m^2/g	133.4	76.5	114.6	39.2
S_{Micro}	m^2/g	28.5	16.1	21.6	10.2
S_{Meso}	m^2/g	105.0	60.4	93.0	29.0
V_{Total}	cm^3/g	0.237	0.219	0.159	0.136
V_{Micro}	cm^3/g	0.026	0.011	0.007	0.003
V_{Meso}	cm^3/g	0.211	0.208	0.143	0.133
$\%V_{Meso}$	%	89.0	99.5	95.3	95.6
Average pore size	nm	6.16	11.12	5.24	14.00

Table 2 The corresponding adsorption kinetic model parameters.

model		Adsorbent	
		HSBC-600	PSBC-600
1. pseudo-first-order			
q_e	mg/g	52.2	21.6
k_1	1/min	0.097	0.063
R^2	-	0.961	0.964
2. pseudo-second-order			
q_e	mg/g	54.5	22.9
k_2	g/(mg·min)	0.003	0.004
h	mg/(g·min)	8.9	2.1
R^2	-	0.994	0.990
3. intra-particle diffusion			
k_{ip1}	mg/g·min$^{0.5}$	5.3	3.0
C_1	mg/g	15.6	1.1
R^2	-	0.991	0.848
k_{ip2}	mg/g·min$^{0.5}$	1.5	0.8
C_2	mg/g	36.8	12.6
R^2	-	0.780	0.805
k_{ip3}	mg/g·min$^{0.5}$	0.07	0.13
C_3	mg/g	52.1	19.2
R^2	-	0.994	0.929

Table 3 The corresponding adsorption isotherm model parameters.

Adsorbent	T (K)	Langmuir model			Freundlich model		
		q_{max} (mg/g)	K_L (L/mg)	R^2	K_F (mg/g)(L/mg)$^{1/n}$	n	R^2
HSBC-600	288	98.0	0.123	0.943	34.9	5.26	0.989
	298	116.9	0.103	0.962	38.8	5.01	0.968
	308	168.3	0.058	0.972	39.6	3.94	0.978
PSBC-600	288	85.0	0.011	0.975	5.1	2.25	0.993
	298	89.3	0.016	0.953	8.2	2.56	0.988
	308	120.3	0.016	0.983	10.8	2.54	0.990

Table 4 The corresponding adsorption thermodynamic parameters.

Adsorbent	T (K)	ΔG^0 (kJ/mol)	ΔH^0 (kJ/mol)	ΔS^0 (J·mol^{-1}·K^{-1})
HSBC-600	288	-10.4	32.6	149.0
	298	-11.6		
	308	-13.4		
PSBC-600	288	-1.6	26.7	98.5
	298	-2.9		
	308	-3.5		